Final Draft
of the original manuscript

Hua, K.; Zhang, Y.; Gan, W.; Kou, H.; Li, J.; Esling, C.:
Correlation between imposed deformation and transformation lattice strain on α variant selection in a metastable β-Ti alloy under isothermal compression.

Correlation between imposed deformation and transformation lattice strain on α variant selection in a metastable β-Ti alloy under isothermal compression

Ke Hua [a, b, c], Yudong Zhang [b, c, *], Weimin Gan [d], Hongchao Kou [a, **], Jinshan Li [a, ***], Claude Esling [b, c]

[a] State Key Laboratory of Solidification Processing, Northwestern Polytechnical University, 710072, Xi'an, PR China
[b] Université de Lorraine, CNRS, Arts et Métiers ParisTech, LEM3, F-57000, Metz, France
[c] Laboratory of Excellence on Design of Alloy Metals for low-mAss Structures (DAMAS), Université de Lorraine, 57073, Metz, France
[d] German Engineering Materials Science Center at MLZ, Helmholtz-Center Geesthacht, D-85748, Garching, Germany

Many phase transformations produce crystallographic variants. Under a mechanical constraint, certain variants could be selected. Although efforts have been made on resolving the selection rule, the trans formation lattice deformation associated selection mechanism has not been well addressed. Thus in the present work, α variant selection of the β to α transformation in a metastable β Ti alloy under compression was studied. Results show that the selection of the α variants is strongly affected by the imposed strain and the applied load with dependence on the local crystal perfection of the β grains. In the slightly deformed β grains, 2 Burger orientation relationship (BOR) variants forming 'cross shaped' clusters and interrelated by a 90° rotation around the $<1\ 1.38\ 2.38\ 0>_\alpha$ axis are selected and form in large quantities (group I variants). Such variants consume the maximum deformation work by the applied load. This energy consumption is rooted from the maximum strain contribution of the selected variants to the macroscopic deformation and the maximum shear stress from the external load resolved on their $\{112\}_\beta < 111 >_\beta$ systems for transformation. In the heavily deformed β grains occupied by dislocation slip bands, several numbers (2 4) of BOR variants are selected but form in much less quantities (group II variants). The selection energy criterion is still obeyed by the group II variants but with restriction from the local deformation. The present work provides clear information on the interweaving of the imposed compression with the internal lattice deformation and its impact on the β to α transformation variant selection.

1. Introduction

For phase transformation in solid state, a specific orientation relationship (OR) between the parent phase and the product phase is present in many metals and alloys, e.g. Fe based alloys (steels) [1−5], Ni Mn based intermetallic compounds [6−8], Zirconium alloys [9,10] and Titanium alloys [11−14]. Due to the symmetry of the parent and the product phase and the OR, the product phase can be represented with a fixed number of crystallographic orien tation variants. When only a small subset of the variants is formed preferentially within one the parent crystal, variant selection oc curs. Since variant selection plays an important role in determining the transformation texture and the final mechanical properties of the material [15−21] and is sensible to many external factors relating to the treatment processes [20,21], study on variant se lection under different external conditions has been intensive. The β to α phase transformation in Ti alloys is a frequent topic for such investigations.

The previous investigations have evidenced that α variant se lection happens in both thermal and thermomechanical processes. The selection could be induced by both internal materials factors

and external treatment factors. For the internal factors, the crystallographic orientation of the β grains and the strain field of certain crystal defects (dislocations) could lead to the selection of grain boundary α ($α_{GB}$) [22−30] and intragranular α precipitates [31−39]. For example for the grain boundary α, if the adjacent β grains share a common $\{110\}_β$ plane within an angular deviation of 10°, the variants with their $\{0001\}_α$ parallel to the common $\{110\}_β$ will form preferentially [22,26,28]. For the intragranular α precipitates, it was found that the $\{1\overline{12}\}_β < \overline{11}\overline{1} >_β$ dislocations produced by cold deformation are in favor of the formation of the α variants with their $(1\overline{1}00)_α$ plane parallel to the slip plane and the $[11\overline{2}0]_α$ parallel to the slip direction [31−33]. It was also revealed by theoretical simulations [32,35] and experimental examinations [36−38] that the annihilation of the transformation lattice strain of certain variants by certain others leads to α variant selection even during a stress free transformation process. Such a selection mechanism well explains the formation of the specific triangular microstructure patterns formed by 3 α variants interrelated by a 60° rotation around their common $< 11\overline{2}0 >_α$ axis. Among the possible external factors, the imposed external deformation is an important and an effective factor to affect variant selection due to the specific lattice deformation of the β to α phase transformation. Investigations through examining the global transformation texture features have evidenced that either under a direct external deformation or a prior deformation (deformation happened before the transformation) the number of intragranular α variants is reduced depending on the slip system activated in the plastic deformation [40−43]. To reveal variant selection within individual β grains under an external deformation, the 3 D phase field simulation has been conducted. Results show that under a compressive pre strain along the $[010]_β$ of a β grain, 4 variants can be selected but under tension, 8 variants can be selected [35].

Despite the numerous theoretical and experimental investigations, the possible interplay between the imposed external deformation and the internal transformation lattice deformation is still not clearly addressed. The reported selection mechanisms stay applicable for individual situations. Based on such an observation, we conducted a thorough investigation, with statistical significance, on variant selection in a metastable β Ti alloy (Ti 7Mo 3Nb 3Cr 3Al) under uniaxial isothermal compression. Special attention was paid to the interplay between the transformation strain and the imposed strain and the applied load. A single β microstructure was obtained as the initial state of the alloy to ensure a stress free initial environment for the β to α phase transformation. A moderate deformation (30% in reduction) and a moderate deformation temperature (700 °C) were applied to provide sufficient imposed strain but to avoid α globularization. This study is expected to work out the underlying mechanism of phase transformation variant selection that could be generalized to other alloys.

2. Experimental procedure and details

The material used in this study is a forged Ti 7333 alloy with the nominal chemical composition of Ti 7Mo 3Nb 3Cr 3Al (wt. %) and the β transus temperature of about 850 °C [44]. Cylindrical specimens with dimensions of Φ10 × 15 mm were cut out of the forged bar and solution treated at 900 °C for 30 min and quenched in water to retain the single β phase by preventing the β to α transformation.

The solution treated specimens were isothermally hot compressed, using a Gleeble 3500 thermo mechanical simulator under vacuum. The specimen was first heated to 700 °C, the compression temperature, at a rate of 25 °C/s and held for 5 s to homogenize the temperature. Then they were compressed at a strain rate of 10^{-3}

s^{-1} to a reduction of 30% and quenched in ice water to preserve the deformed microstructure. A thermocouple was welded at the mid span of the specimens to measure the temperature. Two pieces of thin tantalum sheets were placed between the specimen and the compression die to reduce the friction and maintain a uniform deformation. For comparison, the same initially solution treated specimens were aged under the same heating, isothermal holding and cooling conditions.

The microstructural features of the specimens were examined by scanning electron microscopy electron backscatter diffraction (SEM EBSD), using a JEOL 6500F SEM equipped with an EBSD acquisition camera and the Aztech online acquisition software package (Oxford Instruments). To achieve the surface quality for EBSD measurements, the specimens were first mechanically polished and then electrolytically polished with a solution of 10% perchloric acid in methanol at 35 V for 5 s at a temperature lower than 5 °C. The EBSD measurements were conducted both automatically and manually. The automatic measurements were performed under the beam controlled mode with a step size of 2 μm for the global measurements in an area of about 1.5 × 1.2 mm^2 and with a step size of 70 nm for the local fine measurements. The 1.5 × 1.2 mm^2 area corresponds to the maximum cross section area of homogeneous deformation zone in the compressed specimen. The detailed microstructural features, such as α precipitates and dislocations, were examined by transmission electron microscopy (TEM), using a Philips CM 200 equipped with a LaB6 cathode, a Gatan Orius 833 CCD camera, and the homemade automatic orientation analysis software − Euclid's Phantasies (EP) [45]. The TEM thin films were prepared first by mechanical thinning and then electrolytic polishing to perforation in a solution of 5% perchloric acid in ethanol at a voltage of 35V and at temperatures lower than 35 °C, using a Struers Tenupol 5 twin jet electropolisher.

The lattice constants of the constituent phases at the deformation or the aging temperature (700 °C) were measured in situ by neutron diffraction under vacuum. The through volume measurements were performed with the neutron diffractometer STRESS SPEC located at a thermal beam port of FRM II in Garching, Germany. The Ge (311) monochromator was selected to produce neutrons with a wavelength of 1.618 Å. The $(110)_β$ and $(100)_α$; $(002)_α$; $(101)_α$ diffraction peaks were recorded at $2θ$ 41° with a detector window of 15°. The software StressTextureCalculator (STeCa) [46] was used to extract the diffraction patterns.

Orientation relationships (OR) between the constituent phases were analyzed by misorientation calculation using the measured orientations by SEM EBSD. The dislocations were identified, using the method developed by our group [47]. The β to α transformation associated lattice strain was quantified using displacement gradient tensor.

3. Results

3.1. Initial microstructure

Fig. 1 shows the initial as solution treated microstructure of the Ti 7333 alloy. It is composed of single β phase in the form of equiaxed grains with an average size of about 250 μm. Such a microstructure is typical of metastable β Ti alloys [48−50].

The lattice constants of the β phase and the α phase at 700 °C (the compression and the aging temperature of the present work) are a 3.2471 Å for the β phase (BCC structure), and a 2.9340 Å and c 4.6795 Å for the α phase (HCP structure), respectively. These results will be used later to analyze the lattice deformation of the β to α phase transformation.
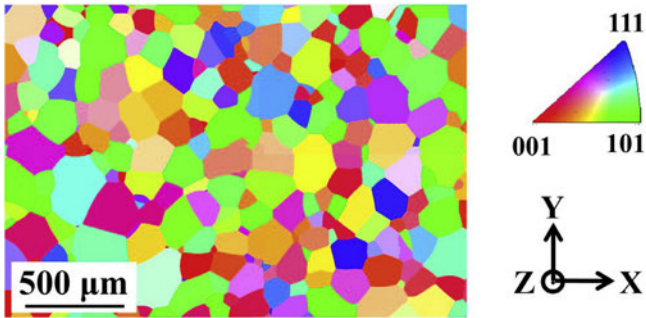
Fig. 1. SEM-EBSD Y axis inverse pole figure (IPF) micrograph of the solution-treated Ti-7333 alloy. Y is parallel to the axial axis of the cylindrical specimen.

3.2. Phase transformation and α variant selection in stress free state

Fig. 2 displays the microstructures and the pole figures of the β and the α phase in the 700 °C aged specimen. It is seen that for the aged specimen three typical α constituents, i.e. α_{GB}, α_W and intra granular α [51,52], are formed (Fig. 2(a)). As the present work fo cuses on variant selection in a homogeneous environment, only the intragranular α is considered. The α_{GB} and α_W are excluded as there exist additional influences from grain boundaries. Further orien tation analyses show that the intragranular α obeys the BOR with the β matrix (Fig. 2(c)) and the α/β interfaces are close to the {11 11 13}$_\beta$, as reported in the literature [26,30]. Globally, there are 12 BOR α variants in each β grain (denoted V1 − V12, as detailed in Table A1 in Appendix), as indicated in Fig. 2(b) and (c). However, locally 3 specific variants form the characteristic triangular clusters, as outlined with the black rectangle in Fig. 2(b). These three variants are interrelated by a 60° rotation around the $<11\bar{2}0>_\alpha$ axis, as illustrated with the $<11\bar{2}0>_\alpha$ pole figures in Fig. 2(d). The for mation mechanisms of the triangular variant clusters in pure Ti and Ti alloys have been thoroughly studied [35−37,44]. It turns out that such a variant organization can efficiently minimize the local transformation strain [37].

3.3. Phase transformation and α variant selection under isothermal compression

Fig. 3 shows the global microstructure of the Ti 7333 alloy after the isothermal compression. It can be seen that the β grains are deformed and elongated (Fig. 3 (a)). Global examination evidenced that the β to α phase transformation happened selectively in the β grains, especially for the intragranular α precipitates, which is in contrast to that in the aged specimen where the transformation is
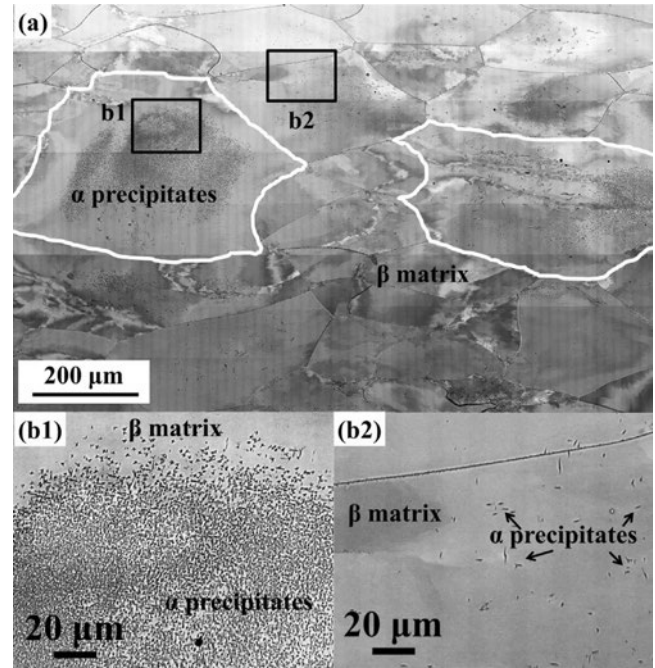

Fig. 3. **(a)** BSE micrograph showing the global microstructure of Ti-7333 after the isothermal compression at 700 °C to a reduction of 30% at a strain rate of 10^{-3} s^{-1}. **(b1)** and **(b2)** the magnified micrographs of the two kinds of representative α precipitates outlined with the black frames in (a).
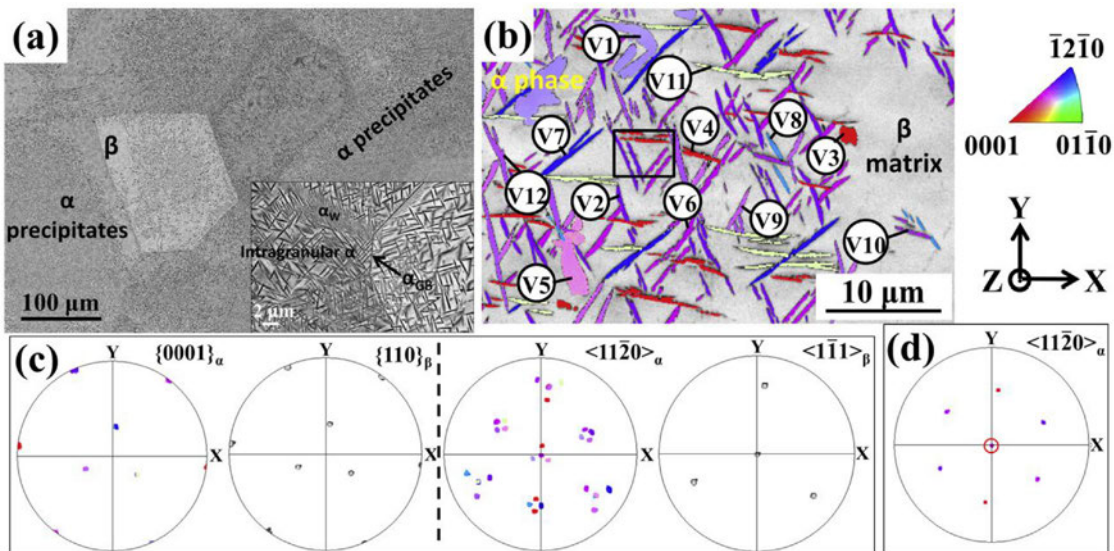

Fig. 2. **(a)** BSE micrograph of the 700° aged Ti-7333 alloy. The insert is a magnified micrograph showing grain boundary α (α_{GB}), Widmanstatten α (α_W) and intragranular α. **(b)** EBSD micrograph (β in band quality contrast; α in Y axis IPF micrograph. Y is the axial axis of the cylindrical specimen) demonstrating the triangular structured intragranular α clusters in the 700 °C aged specimen and the 12 orientation variants denoted V1 V12. **(c)** BOR plane and direction pole figures of the 12 α variants and the β matrix in (b). **(d)** $<11\bar{2}0>_\alpha$ pole figures of the 3 α variants forming the triangular structure enclosed in the black rectangle in (b).

relatively homogeneous. For easy reference, we classify the intragranular α precipitates into two categories: group I and group II. In the former, large amount of intragranular α precipitates appear in the central area of the β grains, as shown in Fig. 3 (b1), whereas in the latter, the α precipitates appear occasionally in the β grain interiors, as shown in Fig. 3 (b2). The transformation is heavily affected by the deformation.

Detailed microstructural examinations revealed that for the group I α precipitates they are still in plate shape but with much smaller sizes with respect to those in the aged specimen, inferring that the imposed strain is effective in refining the precipitates. In addition, the group I α precipitates always tend to agglomerate in the center region of the β grains (Fig. 3 (a)). Close examinations revealed that the group I α plates are oriented in two directions, forming the characteristic 'cross shaped' clusters with the one variant intersecting the other, as shown in Fig. 4 (a). Detailed crystallographic analysis using the SEM EBSD orientation data revealed that the two α plates (as indicated in Fig. 4(a) with their EBSD Kikuchi line diffraction patterns in Fig. 4 (b) still obey the BOR with the parent β grain, as shown with the OR plane and direction pole figures in Fig. 4 (c)). The two variants are interrelated by a 90° rotation around the $<1\ 1.38\ \overline{2.38}\ 0>_\alpha$ axis. Statistical analysis showed that the selected variant pair is either V6 V8 or V7 V12 in one β grain. This result demonstrates that strong variant selection occurred for the group I α precipitates.

For the group II α precipitates, they are mainly distributed in the more deformed and elongated β grains. It should be noted that the quantity of the α precipitates in this group is very low. This indicates that the deformation of the β grains impedes the β to α phase transformation and thus there exists a strong competition between the deformation of the β matrix and its phase transformation. This will be analyzed in detail later. The group II α precipitates are still in plate shape. Crystallographic analysis showed that they still obey the BOR with the parent β grain. In contrast, the numbers of the variants are not consistent, varying from 2 to 4 from one β grain to another. This result still implies that variant selection also happened during the compression. When the grain contains only 2 variants, the 2 variants possess the same disorientation as those in group I, i.e., interrelated by a 90° rotation around the $<1\ 1.38\ \overline{2.38}\ 0>_\alpha$ axis. However, when 3 or 4 variants are precipitated in one β grain, the orientation relationships between the variants are changed to $60°/<11\overline{2}0>_\alpha$, $60.832°/<\overline{1.3771}\ 2.377\ 0.359>_\alpha$ or $63.2618°/<\overline{1}0\overline{5}\overline{5}\overline{3}>_\alpha$. One example of the group II α precipitates in one β grain is shown in Fig. 5. In this β grain, there appear 3

variants, i.e. V1, V5 and V6 (as shown in Fig. 5(a) with their Kikuchi line diffraction patterns displayed in Fig. 5 (b) and their BOR is displayed with the OR plane and direction pole figures in Fig. 5(c)). The orientation relationship between each pair of the variants is either $60°/<11\overline{2}0>_\alpha$ (V1 V6), $60.832°/<\overline{1.3771}\ 2.377\ 0.359>_\alpha$ (V5 V6) or $63.2618°/<\overline{10}\ 5\ 5\ \overline{3}>_\alpha$ (V1 V5). It should be noted that the microstructural and crystallographic characteristics of the two groups of α precipitates were examined in all β grains in a large sample area (1.5×1.2 mm^2). Their statistical representation was confirmed.

Further TEM examinations showed that dislocation quantities in the β grains with intensive α precipitation (Group I) and with much less precipitation (Group II) are quite different, as shown with the representative TEM micrographs in Fig. 6. In the intensive precipitation regions, few dislocations appear (Fig. 6(a)), whereas in the less precipitation regions, large amount of dislocations organized into dislocation bands (the so called slip bands) are visible (Fig. 6(b)). Further analysis using the method in Ref. [47] evidenced that the dislocations in the slip bands are the $\{110\}_\beta <1\overline{1}1>_\beta$ edge type dislocations. Moreover, it should be noted that no $\{1\overline{1}2\}_\beta$ $<\overline{1}11>_\beta$ dislocations were detected in the present deformed alloy. This result indicates that the dislocation slip in the β grains indeed suppresses the α precipitation.

4. Discussion

4.1. β to α phase transformation induced lattice strain

It is known that the β to α phase transformation requires a crystal structure change from the parent BCC structure to the product HCP structure and a redistribution of the chemical elements. The structure transformation from β to α can be regarded as a kind of crystal deformation, different from the common deformation processes in metallic materials, i.e., dislocation slip and twinning. Such a transformation associated deformation can be fully described by a displacement gradient tensor, as analyzed in detail in our previous work [44]. Table 1 displays the displacement gradient tensor of each BOR α variant expressed in the BOR reference frame. From the tensor, we can see that the structure transformation is indeed composed of several strain components: 3 normal strains, i.e., a contraction in the $[1\overline{1}2]_\beta$ direction (ε_{11}), an elongation in the $[\overline{1}1\overline{1}]_\beta$ (ε_{22}) and in the $[110]_\beta$ direction (ε_{33}), and a
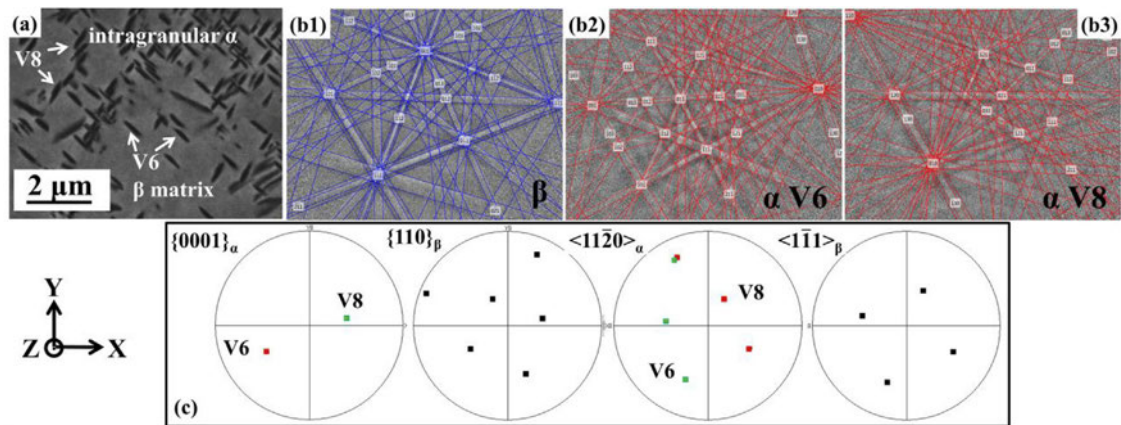

Fig. 4. **(a)** BSE micrograph demonstrating the 'cross-shaped' clusters of the group I intragranular α precipitates; **(b1)**, **(b2)** and **(b3)** the experimental EBSD Kikuchi patterns with the calculated patterns of the β matrix and the two α variants indicated in (a); **(c)** the corresponding BOR plane and direction pole figures of the two selected α variants (V6 and V8) and the surrounding β matrix.
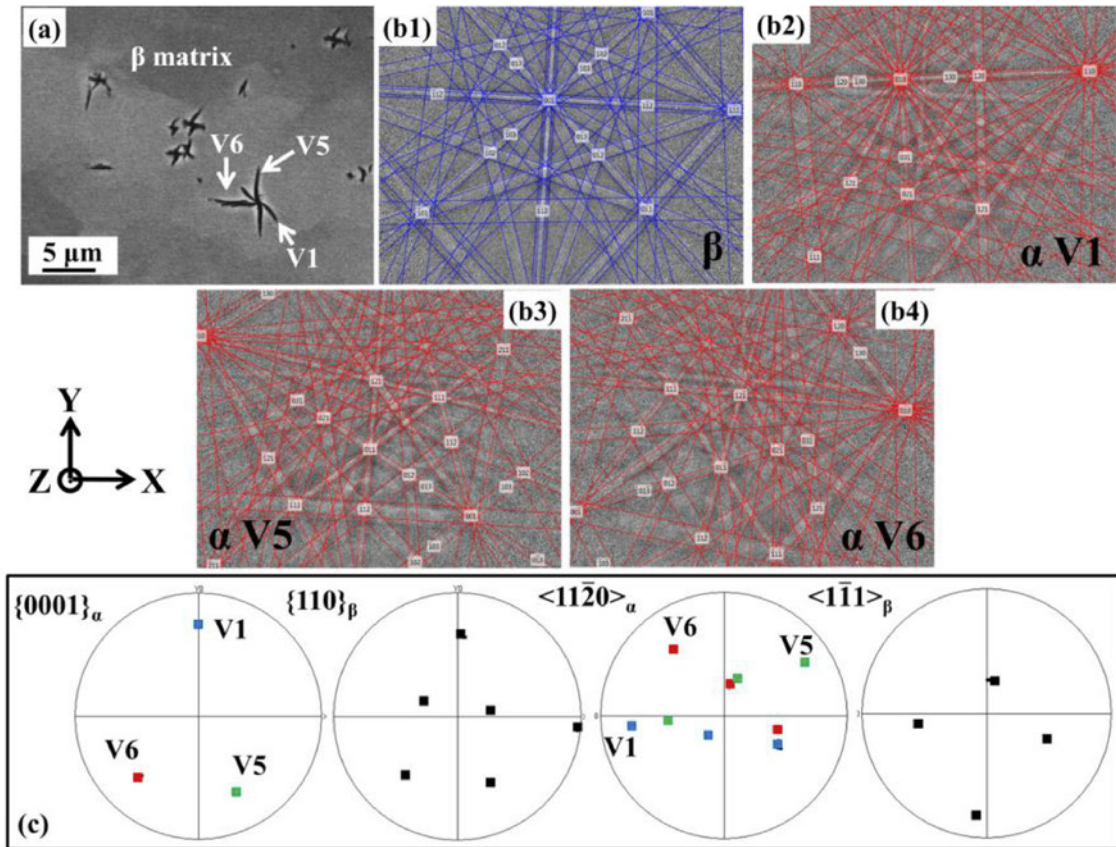
Fig. 5. (a) BSE micrograph demonstrating the group II α precipitates; (b1), (b2) (b3) and (b4) the experimental EBSD Kikuchi patterns with the calculated patterns of the β matrix and the α variants V1, V5 and V6 in (a); (c) the corresponding BOR plane and direction pole figures of the β matrix and the three α variants.
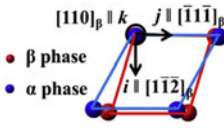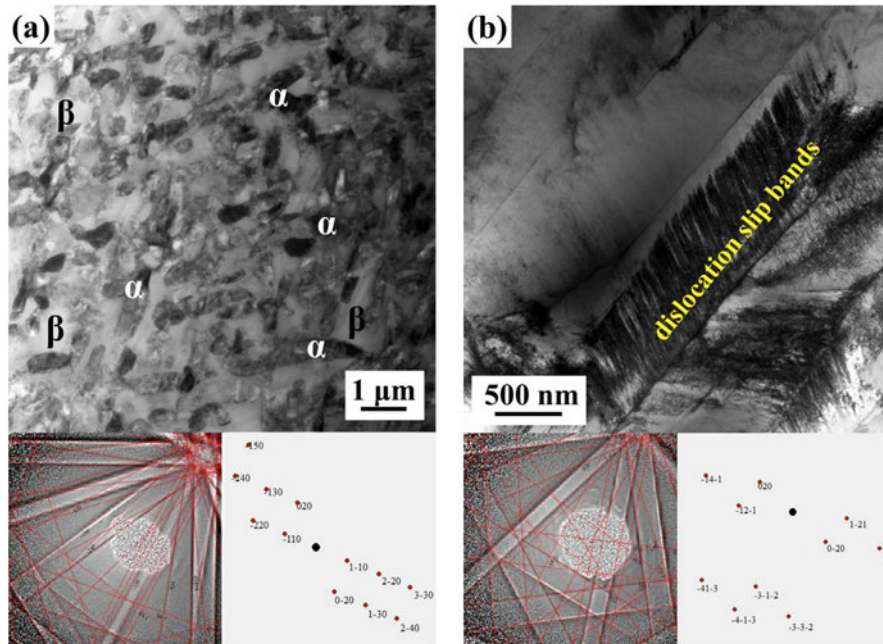

Fig. 6. TEM bright field images showing (a) few dislocations in the β regions with large amount of α precipitates and (b) few α precipitates in the β regions containing large amount of dislocation slip bands. The acquired transmission Kikuchi diffraction patterns and the corresponding calculated spot patterns are displayed in the figures.

Table 1
Displacement gradient tensor of the variant expressed in its BOR reference frame $((110)_\beta//(0001)_\alpha$ and $[\bar{1}1\bar{1}]_\beta//[11\bar{2}0]_\alpha)$.

OR reference frame	Displacement gradient tensor
$[110]_\beta \parallel k$, $j \parallel [\bar{1}1\bar{1}]_\beta$ • β phase • α phase $i \parallel [1\bar{1}\bar{2}]$	$\begin{pmatrix} -0.0416 & 0 & 0 \\ -\mathbf{0.1844} & 0.0434 & 0 \\ 0 & 0 & 0.0189 \end{pmatrix}$

shear on the $(1\bar{1}2)_\beta$ plane and in the $[1\bar{1}1]_\beta$ direction (ε_{21}). Obviously the shear strain component is the largest among all the components for the structure transformation. Interestingly, the shear system ($\{1\,\overline{12}\}_\beta < \overline{11}1 >_\beta$) is also a well recognized slip system in BCC crystals. Thus the most favorable variants should be the ones consume the maximum deformation work under the external compressive load.

In the present work, the deformation work U of the α variants is evaluated following the Patel and Cohen method [53], i.e.,

$$U\left(\sum_p \sigma^p \delta^p + \sum_q \tau^q s^q\right),$$ where σ^p is the resolved normal stress from

the applied load along the respective three principle axes of the BOR reference system, δ^p the normal strain in the corresponding direction, τ^q the shear stress along the principle axis and in a planes perpendicular to the axis and s^q the corresponding shear strain. For simplicity, we assume that the β grains behave like a Sachs aggregate having the local microscopic stress state being identical to the

applied compressive stress and we normalized the magnitude of the applied stress to 1, as treated in Ref. [54]. Then the deformation work U of all the 12 possible variants in each β grain by the external load was calculated in their BOR reference systems to figure out the selection criterion. The analyses were conducted for the α precipitates in the two groups as detailed below.

4.2. Origin of α variant selection in group I

With the measured orientations of the β grains, we calculated the deformation energy of all the 12 possible α variants in each β grain in the observed area (containing 15 grains in the observed area of 1.5×1.2 mm^2. The size of the grain is about 250 μm). Table 2 displays an example of the deformation work of the 12 BOR α variants from one parent β grain and the corresponding stress tensors expressed in the BOR frame of each variant. The experimentally observed (or selected) variants are highlighted in bold. It is seen that among the 12 BOR variants, only V6 and V8 have positive deformation work $U>0$, inferring that the formation of these variants can consume the maximum imposed work of the macroscopic compression and thus they are preferentially selected, whereas the deformation work of the other variants (V1, V2, V3, V4, V5, V7, V9, V10, V11 and V12) are all negative, suggesting that the formation of these variants are not energetically favored by the macroscopic deformation. Between the two selected variants, V6 possesses the higher deformation energy. This variant should be energetically more advantageous. Our microstructure observation indeed confirmed the appearance of the two variants and the dominant occurrence of V6.

To elucidate the interplay of the macroscopic deformation

Table 2
One example of applied stress tensors and deformation work of the 12 possible BOR α variants in one β grain within group I α precipitates. The tensors of the applied stress are expressed in the BOR frame of the corresponding α variant.

No.	Variant	Applied stress tensor	Deformation work
V1	$(110)_\beta//(0001)_\alpha\ [\bar{1}1\bar{1}]_\beta//[11\bar{2}0]_\alpha$	$\begin{pmatrix} -0.0020 & 0.0183 & 0.0405 \\ 0.0183 & -0.1689 & -0.3750 \\ 0.0405 & -0.3750 & -0.8282 \end{pmatrix}$	−0.0263
V2	$(110)_\beta//(0001)_\alpha\ [\bar{1}11]_\beta//[11\bar{2}0]_\alpha$	$\begin{pmatrix} -0.1396 & 0.0670 & 0.3401 \\ 0.0670 & -0.0321 & -0.1632 \\ 0.3401 & -0.1632 & -0.8282 \end{pmatrix}$	−0.0263
V3	$(\bar{1}10)_\beta//(0001)_\alpha\ [111]_\beta//[11\bar{2}0]_\alpha$	$\begin{pmatrix} -0.4761 & 0.4324 & 0.2499 \\ 0.4324 & -0.3927 & -0.2269 \\ 0.2499 & -0.2269 & -0.1311 \end{pmatrix}$	−0.0795
V4	$(\bar{1}10)_\beta//(0001)_\alpha\ [11\bar{1}]_\beta//[11\bar{2}0]_\alpha$	$\begin{pmatrix} -0.1302 & 0.3101 & 0.1307 \\ 0.3101 & -0.7387 & -0.3112 \\ 0.1307 & -0.3112 & -0.1311 \end{pmatrix}$	−0.0863
V5	$(0\bar{1}1)_\beta//(0001)_\alpha\ [111]_\beta//[11\bar{2}0]_\alpha$	$\begin{pmatrix} -0.0010 & -0.0197 & -0.0244 \\ -0.0197 & -0.3927 & -0.4880 \\ -0.0244 & -0.4880 & -0.6063 \end{pmatrix}$	−0.0248
V6	$(\bar{1}01)_\beta//(0001)_\alpha\ [1\bar{1}1]_\beta//[11\bar{2}0]_\alpha$	$\begin{pmatrix} \mathbf{-0.6567} & \mathbf{-0.4039} & \mathbf{0.3375} \\ \mathbf{-0.4039} & \mathbf{-0.1698} & \mathbf{-0.1716} \\ \mathbf{0.3375} & \mathbf{-0.1716} & \mathbf{-0.1735} \end{pmatrix}$	**0.0782**
V7	$(011)_\beta//(0001)_\alpha\ [1\bar{1}1]_\beta//[11\bar{2}0]_\alpha$	$\begin{pmatrix} -0.5866 & 0.3156 & 0.3780 \\ 0.3156 & -0.1698 & -0.2034 \\ 0.3780 & -0.2034 & -0.2436 \end{pmatrix}$	−0.0458
V8	$(101)_\beta//(0001)_\alpha\ [11\bar{1}]_\beta//[11\bar{2}0]_\alpha$	$\begin{pmatrix} \mathbf{-0.2441} & \mathbf{-0.4246} & \mathbf{0.0649} \\ \mathbf{-0.4246} & \mathbf{-0.7387} & \mathbf{0.1129} \\ \mathbf{0.0649} & \mathbf{0.1129} & \mathbf{-0.0173} \end{pmatrix}$	**0.0561**
V9	$(011)_\beta//(0001)_\alpha\ [11\bar{1}]_\beta//[11\bar{2}0]_\alpha$	$\begin{pmatrix} -0.0321 & -0.1748 & 0.1281 \\ -0.1748 & -0.9506 & 0.0236 \\ 0.1281 & 0.0236 & -0.0173 \end{pmatrix}$	−0.0080
V10	$(101)_\beta//(0001)_\alpha\ [\bar{1}11]_\beta//[11\bar{2}0]_\alpha$	$\begin{pmatrix} -0.6177 & 0.1145 & -0.0657 \\ 0.1145 & -0.1387 & 0.4242 \\ -0.0657 & 0.4242 & -0.2436 \end{pmatrix}$	−0.0060
V11	$(\bar{1}01)_\beta//(0001)_\alpha\ [111]_\beta//[11\bar{2}0]_\alpha$	$\begin{pmatrix} -0.5616 & 0.1078 & -0.4682 \\ 0.1078 & -0.0321 & 0.1396 \\ -0.4682 & 0.1396 & -0.4063 \end{pmatrix}$	−0.0056
V12	$(01\bar{1})_\beta//(0001)_\alpha\ [\bar{1}11]_\beta//[11\bar{2}0]_\alpha$	$\begin{pmatrix} -0.0019 & -0.1139 & -0.2743 \\ -0.1139 & -0.9898 & -0.2610 \\ -0.2743 & -0.2610 & -0.0083 \end{pmatrix}$	−0.0220

Table 3
Displacement gradient tensors of the 12 possible BOR α variants in one β grain within group I α precipitates expressed in the sample coordinate system and the resolved shear stress $\tau_{\{1\bar{1}2\}_\beta < \bar{1}1\bar{1}>_\beta}$ on $\{1\bar{1}2\}_\beta <\bar{1}1\bar{1}>_\beta$.

| No.	Variant	Displacement gradient tensor	$\tau_{\{1\bar{1}2\}_\beta < \bar{1}1\bar{1}>_\beta}$
V1	$(110)_\beta//(0001)_\alpha\ [\bar{1}1\bar{1}]_\beta//[11\bar{2}0]_\alpha$	$\begin{pmatrix} 0.0899 & -0.0128 & -0.0830 \\ -0.0467 & 0.0251 & 0.0570 \\ 0.0848 & -0.0115 & -0.0969 \end{pmatrix}$	0.0183
V2	$(110)_\beta//(0001)_\alpha\ [\bar{1}11]_\beta//[11\bar{2}0]_\alpha$	$\begin{pmatrix} 0.0896 & -0.0431 & 0.0678 \\ -0.0092 & 0.0223 & -0.0052 \\ -0.0999 & 0.0633 & -0.0939 \end{pmatrix}$	0.0670
V3	$(\bar{1}10)_\beta//(0001)_\alpha\ [111]_\beta//[11\bar{2}0]_\alpha$	$\begin{pmatrix} 0.0291 & 0.0356 & -0.0253 \\ 0.0202 & 0.0787 & -0.0402 \\ 0.0414 & 0.1309 & -0.0898 \end{pmatrix}$	0.4324
V4	$(\bar{1}10)_\beta//(0001)_\alpha\ [11\bar{1}]_\beta//[11\bar{2}0]_\alpha$	$\begin{pmatrix} 0.0290 & 0.0215 & 0.0346 \\ 0.0369 & 0.0855 & 0.1150 \\ -0.0321 & -0.0561 & -0.0965 \end{pmatrix}$	0.3101
V5	$(0\bar{1}1)_\beta//(0001)_\alpha\ [111]_\beta//[11\bar{2}0]_\alpha$	$\begin{pmatrix} -0.0809 & 0.0014 & 0.0521 \\ -0.1016 & 0.0257 & 0.0605 \\ -0.0914 & 0.0080 & 0.0752 \end{pmatrix}$	−0.0197
V6	$(\bar{1}01)_\beta//(0001)_\alpha\ [1\bar{1}1]_\beta//[11\bar{2}0]_\alpha$	$\begin{pmatrix} \mathbf{0.0401} & \mathbf{0.1033} & \mathbf{0.0896} \\ \mathbf{-0.0151} & \mathbf{-0.0690} & \mathbf{-0.0777} \\ \mathbf{0.0128} & \mathbf{0.0409} & \mathbf{0.0569} \end{pmatrix}$	**−0.4039**
V7	$(011)_\beta//(0001)_\alpha\ [1\bar{1}\bar{1}]_\beta//[11\bar{2}0]_\alpha$	$\begin{pmatrix} -0.0707 & -0.1425 & 0.0561 \\ 0.0098 & 0.0449 & -0.0132 \\ -0.0349 & -0.0633 & 0.0438 \end{pmatrix}$	0.3156
V8	$(101)_\beta//(0001)_\alpha\ [1\bar{1}\bar{1}]_\beta//[11\bar{2}0]_\alpha$	$\begin{pmatrix} \mathbf{0.0291} & \mathbf{-0.0002} & \mathbf{-0.0102} \\ \mathbf{0.1367} & \mathbf{-0.0467} & \mathbf{-0.1077} \\ \mathbf{-0.0345} & \mathbf{0.0133} & \mathbf{0.0456} \end{pmatrix}$	**−0.4246**
V9	$(011)_\beta//(0001)_\alpha\ [1\bar{1}1]_\beta//[11\bar{2}0]_\alpha$	$\begin{pmatrix} -0.0805 & 0.0211 & -0.0448 \\ -0.1312 & 0.0562 & -0.0663 \\ 0.0462 & -0.0162 & 0.0424 \end{pmatrix}$	−0.1748
V10	$(101)_\beta//(0001)_\alpha\ [\bar{1}1\bar{1}]_\beta//[11\bar{2}0]_\alpha$	$\begin{pmatrix} 0.0386 & 0.1289 & -0.0414 \\ -0.0080 & -0.0053 & 0.0226 \\ -0.0172 & -0.0984 & 0.0501 \end{pmatrix}$	0.1145
V11	$(\bar{1}01)_\beta//(0001)_\alpha\ [111]_\beta//[11\bar{2}0]_\alpha$	$\begin{pmatrix} 0.0305 & -0.0051 & 0.0097 \\ 0.1134 & -0.0064 & 0.0538 \\ 0.0865 & -0.0648 & 0.0621 \end{pmatrix}$	0.1078
V12	$(01\bar{1})_\beta//(0001)_\alpha\ [\bar{1}11]_\beta//[11\bar{2}0]_\alpha$	$\begin{pmatrix} -0.0716 & -0.1081 & -0.1052 \\ -0.0051 & 0.0266 & 0.0013 \\ 0.0383 & 0.0539 & 0.0730 \end{pmatrix}$	−0.1139
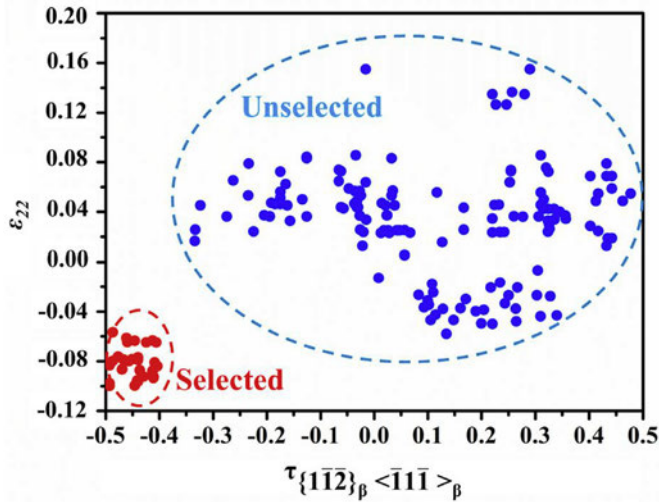
Fig. 7. The resolved shear stress on $\{1\bar{1}2\}_\beta<\bar{1}1\bar{1}>_\beta$ shear system of all the possible group I α variants under the external compressive load and their corresponding ε_{22} values in the observed area (1.5×1.2 mm^2). The active variants consuming positive deformation work are in red, whereas the unselected variants consuming negative work are in blue. (For interpretation of the references to color in this figure legend, the reader is referred to the Web version of this article.)

(strain and applied load) with the lattice deformation of the selected variants that is behind the unique energy criterion and their influence on the morphology of the α precipitates, we further

expressed the lattice deformation of the 12 variants in the sample coordinate system X Y Z as presented in the microstructure figures and calculated the resolved shear stress on the $\{1\bar{1}2\}_\beta<\bar{1}1\bar{1}>_\beta$ shear system. The results are displayed in Table 3 and the experimentally observed (or selected) variants are highlighted in bold. As the Y axis is the compression axis, the elements in the second row of the tensor are of particular importance with respect to the imposed macroscopic compression. $\varepsilon_{22} < 0$ means that the β to α trans formation induces a contraction in the compression direction (Y direction). This contraction is compatible to the macroscopic compression and thus can effectively contribute to the macroscopic deformation. The negative $\tau_{\{1\bar{1}2\}_\beta < \bar{1}1\bar{1}>_\beta}$ implies that the shear stress revolved from the applied load on the $\{1\bar{1}2\}_\beta<\bar{1}1\bar{1}>_\beta$ shear system is in the same direction as that of the shear strain for structure transformation (that is also negative, as given in Table 1). It should be noted that the negative shear ensures a smallest atomic movement for structure transformation, as seen in the figure of the atomic correspondence between the β and the α phase in Table 1. Thus the shear deformation to realize the structure transformation is unidirectional similar to the case of twinning. Only a negative resolved shear stress is possible to active the $\{1\bar{1}2\}_\beta<\bar{1}1\bar{1}>_\beta$ shear system for structure transformation From Table 3, it is seen that the selected variants V6 and V8 satisfy simultaneously the two condi tions, i.e. $\varepsilon_{22} < 0$ and $\tau_{\{1\bar{1}2\}_\beta < \bar{1}1\bar{1}>_\beta} < 0$. Thus the reasons behind the unique deformation energy criterion of the selected variants in Table 2 can be interpreted such that the resolved shear stress $\tau_{\{1\bar{1}2\}_\beta < \bar{1}1\bar{1}>_\beta}$ should be able to activate the $\{1\bar{1}2\}_\beta<\bar{1}1\bar{1}>_\beta$ shear system for the initiation of the transformation, as this shear system

Table 4
One example of applied stress tensors and deformation work of the 12 possible BOR α variants in one β grain within group II α precipitates. The applied stress tensors are expressed in the BOR frame of each α variant.

No.	Variant	Applied stress tensor	Deformation work
V1	$(110)_\beta//(0001)_\alpha\ [\bar{1}1\bar{1}]_\beta//[11\bar{2}0]_\alpha$	$\begin{pmatrix} -0.0777 & -0.0987 & -0.2528 \\ -0.0987 & -0.0992 & -0.2857 \\ -0.2528 & -0.2857 & -0.8232 \end{pmatrix}$	**0.0016**
V2	$(110)_\beta//(0001)_\alpha\ [\bar{1}11]_\beta//[11\bar{2}0]_\alpha$	$\begin{pmatrix} -0.1519 & -0.0615 & 0.3536 \\ -0.0615 & -0.0249 & 0.1431 \\ 0.3536 & 0.1431 & -0.8232 \end{pmatrix}$	0.0010
V3	$(\bar{1}10)_\beta//(0001)_\alpha\ [111]_\beta//[11\bar{2}0]_\alpha$	$\begin{pmatrix} -0.7326 & 0.4329 & 0.0826 \\ 0.4329 & -0.2545 & -0.0485 \\ 0.0826 & -0.0485 & -0.0093 \end{pmatrix}$	−0.0604
V4	$(\bar{1}10)_\beta//(0001)_\alpha\ [11\bar{1}]_\beta//[11\bar{2}0]_\alpha$	$\begin{pmatrix} -0.0360 & 0.1853 & 0.0182 \\ 0.1853 & -0.9548 & -0.0940 \\ 0.0182 & -0.0940 & -0.0093 \end{pmatrix}$	−0.0743
V5	$(0\bar{1}1)_\beta//(0001)_\alpha\ [111]_\beta//[11\bar{2}0]_\alpha$	$\begin{pmatrix} -0.1195 & -0.1744 & -0.2735 \\ -0.1744 & -0.2545 & -0.3991 \\ -0.2735 & -0.3991 & -0.6260 \end{pmatrix}$	**0.0143**
V6	$(\bar{1}01)_\beta//(0001)_\alpha\ [1\bar{1}1]_\beta//[11\bar{2}0]_\alpha$	$\begin{pmatrix} -0.4178 & -0.2585 & -0.4492 \\ -0.2585 & -0.0992 & -0.2188 \\ -0.4492 & -0.2188 & -0.4830 \end{pmatrix}$	**0.0415**
V7	$(011)_\beta//(0001)_\alpha\ [1\bar{1}1]_\beta//[11\bar{2}0]_\alpha$	$\begin{pmatrix} -0.8558 & 0.2913 & 0.1964 \\ 0.2913 & -0.0992 & -0.0669 \\ 0.1964 & -0.0669 & -0.0451 \end{pmatrix}$	−0.0233
V8	$(101)_\beta//(0001)_\alpha\ [11\bar{1}]_\beta//[11\bar{2}0]_\alpha$	$\begin{pmatrix} -0.0317 & -0.1741 & 0.0207 \\ -0.1741 & -0.9548 & 0.1134 \\ 0.0207 & 0.1134 & -0.0135 \end{pmatrix}$	−0.0083
V9	$(011)_\beta//(0001)_\alpha\ [11\bar{1}]_\beta//[11\bar{2}0]_\alpha$	$\begin{pmatrix} -0.2616 & 0.1547 & 0.1138 \\ 0.1547 & -0.7249 & -0.0183 \\ 0.1138 & -0.0183 & -0.0135 \end{pmatrix}$	−0.0494
V10	$(101)_\beta//(0001)_\alpha\ [\bar{1}11]_\beta//[11\bar{2}0]_\alpha$	$\begin{pmatrix} -0.5001 & 0.0112 & 0.0024 \\ 0.0112 & -0.4548 & 0.2075 \\ 0.0024 & 0.2075 & -0.0451 \end{pmatrix}$	−0.0019
V11	$(\bar{1}01)_\beta//(0001)_\alpha\ [111]_\beta//[11\bar{2}0]_\alpha$	$\begin{pmatrix} -0.3491 & -0.0935 & -0.4675 \\ -0.0935 & -0.0249 & -0.1248 \\ -0.4675 & -0.1248 & -0.6260 \end{pmatrix}$	0.0188
V12	$(01\bar{1})_\beta//(0001)_\alpha\ [\bar{1}11]_\beta//[11\bar{2}0]_\alpha$	$\begin{pmatrix} -0.9045 & 0.2086 & -0.3561 \\ 0.2086 & -0.0630 & 0.3506 \\ -0.3561 & -0.3506 & -0.0325 \end{pmatrix}$	−0.0042

is a slip system of the β phase, and the shear amount is very large with respect to the normal strains (as shown in Table 1) and the growth of the variants should make maximum contribution to the macroscopic deformation. Such a compatible stress and strain characterized energy criterion of variant selection has been verified for all the group I α precipitates in the large observation area mentioned above (1.5 × 1.2 mm^2), and the results represented by the ε_{22} values and the $\tau_{\{1\bar{1}2\}_\beta<\bar{1}1\bar{1}>_\beta}$ on the $\{1\bar{1}2\}_\beta<\bar{1}1\bar{1}>_\beta$ shear system are displayed in Fig. 7, where $U > 0$ and $U < 0$ are signified by the respective red and blue colors. As seen in the figure, for the selected variants, the deformation work U is always positive. In detail, they have both the smallest $\tau_{\{1\bar{1}2\}_\beta<\bar{1}1\bar{1}>_\beta}$ (from 0.4 to 0.5) and the smallest ε_{22} values ($\varepsilon_{22} < 0$). For the inactive variants, U is negative and they have either positive $\tau_{\{1\bar{1}2\}_\beta<\bar{1}1\bar{1}>_\beta}$ for the $\{1\bar{1}2\}_\beta<\bar{1}1\bar{1}>_\beta$ shear systems (from 0.02 to 0.35) or the positive ε_{22} (from 0.0127 to 0.155). This statistical result further validates the energy criterion of the variant selection for the group I α precipitates and this energy criterion corresponds to a compatible stress and strain associated selection mechanism, i.e., only the variants that can receive the largest resolved shear stress from the applied compressive load to activate the $\{1\bar{1}2\}_\beta<\bar{1}1\bar{1}>_\beta$ shear system for structure transformation and that can make highest contribution to the macroscopic deformation will be selected. These variants also appear in highest amounts.

It should be noted that any non zero values of ε_{21} and ε_{23} in Table 3 represent shears in the direction of Y (compression direction). These shears increase the dimension of the α precipitates with respect to the original β matrix in this direction, and thus

could be incompatible with the macroscopic compression. The shear components ε_{21} and ε_{23} of V6 and V8 in group I are not zero, meaning that the formation of these variants also induces a dimension increase in the compression direction that cancels, to some extent, the contribution of ε_{22}. However, the dimension in crease induced by the shear strain depends on the thickness of the precipitates in the two direction perpendicular to the compression direction (X and Z direction indicated in Fig. 4). To diminish the negative effect of the two shears, the size of the precipitates should be reduced. Thus the two shears induced by the structure trans formation impede the growth of the α precipitates. The smaller size of the group I precipitates with respect to those formed during aging is indeed confirmed by our microstructure observation.

4.3. Origin of α variant selection in group II

The deformation energy criterion for the selection of the group I precipitates were verified for the group II α precipitates. Table 4 shows the deformation work U of the 12 BOR α variants from one parent β grain and their corresponding applied stress tensors expressed in the BOR frame of each variant. Table 5 displays the lattice deformation of the 12 variants in the sample coordinate system X Y Z and the $\tau_{\{1\bar{1}2\}_\beta<\bar{1}1\bar{1}>_\beta}$ on the $\{1\bar{1}2\}_\beta<\bar{1}1\bar{1}>_\beta$ shear system to further resolve the interplay of the imposed deformation and the applied loads with the transformation deformation. In the two tables the selected variants are highlighted in bold. In this example, there are 5 variants (V1, V2, V5, V6 and V11) satisfying the energy criterion (having the positive work) (Table 4) and the for mation of these variants receives a negative $\tau_{\{1\bar{1}2\}_\beta<\bar{1}1\bar{1}>_\beta}$ (Table 5)

Table 5
Displacement gradient tensors of the 12 possible BOR α variants in one β grain (group II α precipitates) expressed in the sample coordinate system and the resolved shear stress $\tau_{\{1\bar{1}2\}_\beta <\bar{1}1\bar{1}>_\beta}$ on $\{1\bar{1}2\}_\beta <\bar{1}1\bar{1}>_\beta$.

| No.	Variant	Deformation gradient tensor			$\tau_{\{1\bar{1}2\}_\beta <\bar{1}1\bar{1}>_\beta}$
V1	$(110)_\beta//(0001)_\alpha\ [\bar{1}1\bar{1}]_\beta//[11\bar{2}0]_\alpha$	**0.0982**	**0.0227**	**−0.0633**	**−0.0987**
		−0.0537	**−0.0011**	**0.0492**	
		0.1040	**0.0362**	**−0.0794**	
V2	$(110)_\beta//(0001)_\alpha\ [\bar{1}11]_\beta//[11\bar{2}0]_\alpha$	0.1011	−0.0463	0.0872	−0.0615
		0.0301	−0.0023	0.0382	
		−0.0801	0.0511	−0.0808	
V3	$(\bar{1}10)_\beta//(0001)_\alpha\ [111]_\beta//[11\bar{2}0]_\alpha$	0.0171	−0.0033	0.0023	0.4329
		0.0045	0.0598	−0.0100	
		0.0200	0.1733	−0.0588	
V4	$(\bar{1}10)_\beta//(0001)_\alpha\ [11\bar{1}]_\beta//[11\bar{2}0]_\alpha$	0.0173	0.0064	0.0194	0.1853
		−0.0014	0.0736	0.1611	
		0.0017	−0.0222	−0.0728	
V5	$(0\bar{1}1)_\beta//(0001)_\alpha\ [111]_\beta//[11\bar{2}0]_\alpha$	**−0.0343**	**−0.0195**	**0.0125**	**−0.1744**
		−0.1036	**−0.0123**	**0.0354**	
		−0.1334	**−0.0396**	**0.0677**	
V6	$(\bar{1}01)_\beta//(0001)_\alpha\ [1\bar{1}1]_\beta//[11\bar{2}0]_\alpha$	**−0.0082**	**0.0952**	**0.1234**	**−0.2585**
		0.0189	**−0.0325**	**−0.0738**	
		−0.0047	**0.0345**	**0.0687**	
V7	$(011)_\beta//(0001)_\alpha\ [1\bar{1}\bar{1}]_\beta//[11\bar{2}0]_\alpha$	−0.0300	−0.1578	0.0108	0.2913
		−0.0050	0.0226	−0.0044	
		−0.0284	−0.0998	0.0254	
V8	$(101)_\beta//(0001)_\alpha\ [1\bar{1}\bar{1}]_\beta//[11\bar{2}0]_\alpha$	−0.0112	0.0084	0.0146	−0.1741
		0.1690	0.0076	−0.0912	
		−0.0068	−0.0033	0.0217	
V9	$(011)_\beta//(0001)_\alpha\ [1\bar{1}1]_\beta//[11\bar{2}0]_\alpha$	−0.0414	0.0017	−0.0372	0.1547
		−0.1511	0.0395	−0.1000	
		0.0019	−0.0046	0.0199	
V10	$(101)_\beta//(0001)_\alpha\ [\bar{1}1\bar{1}]_\beta//[11\bar{2}0]_\alpha$	0.0031	0.1697	−0.0147	0.0112
		0.0091	−0.0108	−0.0012	
		0.0067	−0.0891	0.0257	
V11	$(\bar{1}01)_\beta//(0001)_\alpha\ [111]_\beta//[11\bar{2}0]_\alpha$	−0.0198	0.0238	−0.0130	−0.0935
		0.1001	−0.0094	0.0466	
		0.1151	−0.0617	0.0772	
V12	$(01\bar{1})_\beta//(0001)_\alpha\ [\bar{1}11]_\beta//[11\bar{2}0]_\alpha$	−0.0198	−0.1011	−0.1409	0.2086
		−0.0169	−0.0199	−0.0497	
		0.0039	0.0253	0.0578	
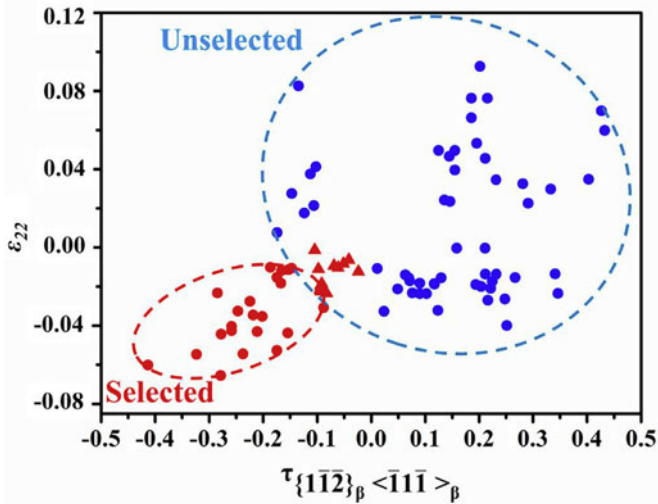
Fig. 8. The resolved shear stress on $\{1\bar{1}2\}_\beta<\bar{1}1\bar{1}>_\beta$ shear systems of all the possible group II α variants under the external compressive load and their corresponding ε_{22} values in the observed area ($1.5 \times 1.2\ mm^2$). The active variants consuming positive deformation work are in red, whereas the unselected variants consuming negative work are in blue. For the unselected variants consuming positive work, they are represented with the red triangles. (For interpretation of the references to color in this figure legend, the reader is referred to the Web version of this article.)

that is prerequisite for the activation of the $\{1\bar{1}2\}_\beta<\bar{1}1\bar{1}>_\beta$ shear system for transformation and provides a contraction in the compression direction, making positive contribution to the macroscopic deformation, however, only 3 variants (V1, V5 and V6) were detected (Tables 4 and 5). Thus, in principle the energy criterion of the selection is respected by the transformation but with restrictions. The energy criterion and the compatible stress and strain characters of the selected variants were further verified with all the group II α precipitates in the whole observation area (containing 9 grains in the observed area of $1.5 \times 1.2\ mm^2$) and the results are displayed in Fig. 8. It is seen that for the selected variants the energy criterion is well respected and the compatible characters of the macroscopic compression with the lattice strain and the $\tau_{\{1\bar{1}2\}_\beta <\bar{1}1\bar{1}>_\beta}$ with the shear strain for transformation are well reproduced. However, there are still some variants that fulfill the energy criteria and possess the compatible characters with the macroscopic deformation that did not appear, as indicated with the red triangles in Fig. 8. For such variants, the resolved shear stress on their $\{1\bar{1}2\}_\beta<\bar{1}1\bar{1}>_\beta$ shear systems and their ε_{22} are very close to the limit (0.0945 to 0.0237 for the $\tau_{\{1\bar{1}2\}_\beta <\bar{1}1\bar{1}>_\beta}$ and 0.0234 to 0.0013 for the ε_{22}), meaning that they receive limited resolved shear stress to activate the $\{1\bar{1}2\}_\beta<\bar{1}1\bar{1}>_\beta$ shear system for phase transformation and provide limited contribution to the macroscopic compression. Moreover, the local environment of the host β grains also exerts strong influence on the formation of such variants. For the group II α precipitates, they are nucleated in the β grains heavily deformed by dislocation slip. As evidenced by the TEM observations (Fig. 6(b)), large amount of $\{110\}_\beta<1\bar{1}1>_\beta$ dislocations exist in the host β grains of the group II α precipitates. Calculation demonstrated that for these β grains the $\{110\}_\beta <1\bar{1}1>_\beta$

slip systems are indeed at the favorable activation position (Schmid Factors >0.42). As the dislocations are organized in slip bands and the bands nearly occupy the entire β grains, we can deduce that dislocation multiplication and dynamic recovery happened intensively during the deformation, and in consequence, the β lattice is largely distorted. Such an environment is unfavorable for the β to α transformation as the phase transformation requires certain crystalline perfection to realize the coordinated atomic movements for the structure change. Thus with the modified local stress and strain state, the formation of the variants with less competitiveness with respect to the external compression is not certain. They can be selected or not selected depending on the local state of the β grain. Thus the selection of the α variants are further restricted by the local stress and strain conditions.

5. Conclusions

Variant selection of intragranular α during isothermal compression in a metastable β Ti alloy was thoroughly investigated by SEM, EBSD and TEM, and analyzed with transformation strain and deformation work in the present work. The interplay between the lattice strain induced by phase transformation and the imposed compressive strain and the applied compressive load was evidenced as the key factor for α variant selection. Based on the experimental observations and theoretical analyses, the following conclusions are drawn:

- A strong variant selection of the intragranular α precipitates occurred during the isothermal compression and the selected variants can be classified into two groups (group I and group II), according to their precipitation amount.
- For the group I α precipitates, the precipitation amount is large and the precipitates are agglomerated in the β grains with fewer dislocations. Only 2 variants forming 'cross shaped' clusters are selected. The 2 variants respect the BOR and are interrelated by a 90° rotation around the $<1\ 1.38\ \overline{2.38}\ 0>_\alpha$ axis. Such variants consume the maximum amount of deformation work by the external compression. This energy criterion can be further interpreted by the compatibility of the microscopic strain to the macroscopic strain and the shear stress resolved from the external load to the local transformation shear deformation. That is the formation of the selected variants offer the maximum contribution to the imposed compression strain and receive the maximum resolved shear stress on the $\{1\overline{12}\}_\beta<\overline{11}1>_\beta$ shear system for the structure transformation.
- For the group II α precipitates, they appear in much smaller numbers and are dispersed in the β grains that are occupied also by large amount of dislocation slip bands. The numbers of the variants in group II are not constant, varying from 2 to 4 from one β grain to another. The selection of the variants still respects the energy criterion for the selection of the group I precipitates and reproduce the same strain and stress compatible characters as the group I precipitates but with restriction from the local stress and strain states imposed by the large amount of dislocations.

The results of the present work reveal in depth the interplay between the lattice strain of the phase transformation and the imposed macroscopic deformation and the applied external load.

References

[1] I. Lischewski, G. Gottstein, Nucleation and variant selection during the α γ α phase transformation in microalloyed steel, Acta Mater. 59 (2011) 1530 1541.
[2] L. Kestens, R. Petrov, Y. Houbaert, Orientation selective martensite transformation in an Fe-28Ni alloy, ISIJ Int. 43 (2003) 1444 1452.
[3] K. Verbeken, L. Kestens, Strain-induced selective growth in an ultra low carbon steel after a small rolling reduction, Acta Mater. 51 (2003) 1679 1690.
[4] M.P. Butrón-Guillén, C.S. Da Costa Viana, J.J. Jonas, A variant selection model for predicting the transformation texture of deformed austenite, Metall. Mater. Trans. 28 (1997) 1755 1768.
[5] L. Kestens, J.J. Jonas, Modeling texture change during the static recrystallization of interstitial free steels, Metall. Mater. Trans. 27 (1996) 155 164.
[6] Y.D. Wang, D.W. Brown, H. Choo, P.K. Liaw, D.Y. Cong, M.L. Benson, L. Zuo, Experimental evidence of stress-field-induced selection of variants in Ni-Mn-Ga ferromagnetic shape-memory alloys, Phys. Rev. B 17 (2007), 174404.
[7] Z.B. Li, B. Yang, Y.D. Zhang, C. Esling, N.F. Zou, X. Zhao, L. Zuo, Crystallographic insights into the intermartensitic transformation in Ni Mn Ga alloys, Acta Mater. 74 (2014) 9 17.
[8] R. Chulist, L. Straka, A. Sozinov, T. Lippmann, W. Skrotzki, Modulation reorientation in 10M Ni-Mn-Ga martensite, Scripta Mater. 68 (2013) 671 674.
[9] J. Romero, M. Preuss, J. Quinta da Fonseca, Texture memory and variant selection during phase transformation of a zirconium alloy, Acta Mater. 57 (2009) 5501 5511.
[10] L. Capolungo, P.E. Marshall, R.J. McCabe, I.J. Beyerlein, C.N. Tomé, Nucleation and growth of twins in Zr: a statistical study, Acta Mater. 57 (2009) 6047 6056.
[11] M. Bonisch, A. Panigrahi, M. Stoica, M. Calin, E. Ahrens, M. Zehetbauer, W. Skrotzki, J. Eckert, Giant thermal expansion and α-precipitation pathways in Ti-alloys, Nat. Commun. 8 (2017) 1429.
[12] M. Bonisch, T. Waitz, M. Calin, W. Skrotzki, J. Eckert, Tailoring the Bain strain of martensitic transformations in TiNb alloys by controlling the Nb content, Int. J. Plast. 85 (2016) 190 202.
[13] S. van Bohemen, A. Kamp, R. Petrov, L. Kestens, J. Sietsma, Nucleation and variant selection of secondary α plates in a β Ti alloy, Acta Mater. 56 (2008) 5907 5914.
[14] N. Stanford, P.S. Bate, Crystallographic variant selection in Ti-6Al-4V, Acta Mater. 52 (2004) 5215 5224.
[15] J.J. Jonas, S.J. Mu, T.A. Samman, G. Gottstein, L. Jiang, E. Martin, The role strain accommodation during the variant selection of primary twins in magnesium, Acta Mater. 59 (2011) 2046 2056.
[16] S.J. Mu, J.J. Jonas, G. Gottstein, Variant selection of primary, secondary and tertiary twins in a deformed Mg alloy, Acta Mater. 60 (2012) 2043 2053.
[17] A. Devaraj, V.V. Joshi, A. Srivastava, S. Manandhar, V. Moxson, V.A. Duz, C. Lavender, A low-cost hierarchical nanostructured beta-titanium alloy with high strength, Nat. Commun. 7 (2016) 11176.
[18] G. Lütjering, J.C. Williams, Titanium, Berlin, Springer Berlin Heidelberg, Heidelberg, 2007.
[19] R.R. Boyer, Attributes, characteristics, and applications of titanium and its alloys, JOM 62 (2010) 21 24.
[20] R. Shi, Variant Selection during Alpha Precipitation in Titanium Alloys: a Simulation Study, Ph.D. thesis, The Ohio State University, 2014.
[21] Y.F. Zheng, R.E.A. Williams, D. Wang, R. Shi, S. Nag, P. Kami, J.M. Sosa, R. Banerjee, Y. Wang, H.L. Fraser, Role of ω phase in the formation of extremely refined intragranular α precipitates in metastable β-titanium alloys, Acta Mater. 103 (2016) 850 858.
[22] T. Furuhara, S. Takagi, H. Watanabe, T. Maki, Crystallography of grain boundary α precipitates in a β titanium alloy, Metall. Mater. Trans. 27 (1996) 1635 1646.
[23] M. Salib, J. Teixeira, L. Germain, E. Lamielle, N. Gey, E. Aeby-Gautier, Influence of transformation temperature on microtexture formation associated with α precipitation at β grain boundaries in a β metastable titanium alloy, Acta Mater. 61 (2013) 3758 3768.
[24] C. Cayron, Importance of the transformation in the variant selection

mechanisms of thermomechanically processed titanium alloys, Scripta Mater. 59 (2008) 570 573.

[25] G. Gottstein, L. Shvindlerman, Grain Boundary Migration in Metals: Thermodynamics, Kinetics, Applications, second ed., Taylor & Francis Group, Boca Raton, 2009.

[26] D. Bhattacharyya, G.B. Viswanathan, H.L. Fraser, Crystallographic and morphological relationships between β phase and the Widmanstatten and allotriomorphic α phase at special β grain boundaries in an α/β titanium alloy, Acta Mater. 55 (2007) 6765 6778.

[27] E. Lee, R. Banerjee, S. Kar, D. Bhattacharyya, H.L. Fraser, Selection of α variants during microstructural evolution in α/β titanium alloy, Phil. Mag. 87 (2007) 3615 3627.

[28] R. Shi, V. Dixit, H.L. Fraser, Y. Wang, Variant selection of grain boundary α by special prior β grain boundaries in titanium alloys, Acta Mater. 75 (2014) 156 166.

[29] R. Shi, V. Dixit, G.B. Viswanathan, H.L. Fraser, Y. Wang, Experimental assessment of variant selection rules for grain boundary α in titanium alloys, Acta Mater. 102 (2016) 197 211.

[30] N. Vanderesse, E. Maire, M. Darrieulat, F. Montheillet, M. Moreaudc, D. Jeulin, Three-dimensional microtomographic study of Widmanstatten microstructures in an alpha/beta titanium alloy, Scripta Mater. 58 (2008) 512 515.

[31] D. Qiu, R. Shi, D. Zhang, W. Lua, Y. Wang, Variant selection by dislocations during a precipitation in α/β titanium alloys, Acta Mater. 88 (2015) 218 231.

[32] C.P. Luo, G.C. Weatherly, The invariant line and precipitation in a Ni-45 wt% Cr alloy, Acta Metall. 35 (1987) 1963 1972.

[33] T. Furuhara, T. Maki, Variant selection in heterogeneous nucleation on defects in diffusional phase transformation and precipitation, Mater. Sci. Eng., A 312 (2001) 145 154.

[34] W.G. Burgers, On the process of transition of the cubic-body-centered modification into the hexagonal-close-packed modification of zirconium, Physica 1 (1934) 561 586.

[35] R. Shi, Y. Wang, Variant selection during α precipitation in Ti 6Al 4V under the influence of local stress a simulation study, Acta Mater. 61 (2013) 6006 6024.

[36] M. Naoki, N. Takahiro, I. Teruhiko, A. Kei, Reasons for formation of triangular α precipitates in Ti 15V 3Cr 3Sn 3Al titanium alloy, Mater. Trans. 47 (2006) 341 347.

[37] S.C. Wang, M. Aindow, M.J. Starink, Effect of self-accommodation on α/α boundary populations in pure titanium, Acta Mater. 51 (2013) 2485 2503.

[38] K. Otsuka, X. Ren, Physical metallurgy of Ti-Ni-based shape memory alloys, Prog. Mater. Sci. 50 (2005) 511 678.

[39] D. He, J.C. Zhu, S. Zaefferer, D. Raabe, Y. Liu, Z.L. Lai, X.W. Yang, Influences of deformation strain, strain rate and cooling rate on the Burgers orientation relationship and variants morphology during phase transformation in a near titanium alloy, Mater. Sci. Eng., A 549 (2012) 20 29.

[40] T. Karthikeyan, A. Dasgupta, R. Khatirkar, S. Saroja, I. Samajdar, M. Vijayalakshmi, Effect of cooling rate on transformation texture and variant selection during β→ α transformation in Ti-5Ta-1.8Nb alloy, Mater. Sci. Eng., A 528 (2010) 549 558.

[41] G.A. Sargent, K.T. Kinsel, A.L. Pilchak, A.A. Salem, S.L. Semiatin, Variant selection during cooling after beta annealing of Ti-6Al-4V ingot material, Metall. Mater. Trans. 43 (2012) 3570 3585.

[42] G.C. Obasi, S. Birosca, D.G. Leo Prakash, J. Quinta da Fonseca, M. Preuss, The influence of rolling temperature on texture evolution and variant selection during phase transformation in Ti 6Al 4V, Acta Mater. 60 (2012) 6013 6024.

[43] Z.S. Zhu, J.L. Gu, N.P. Chen, Variant selection in phase transformation of cold rolled titanium sheet, Scripta Mater. 34 (1996) 1281 1286.

[44] K. Hua, Y.D. Zhang, H.C. Kou, J.S. Li, W.M. Gan, J. Fundenberger, C. Esling, Composite structure of α phase in metastable β Ti alloys induced by lattice strain during β to α phase transformation, Acta Mater. 132 (2017) 307 326.

[45] A. Morawiec, J.J. Fundenberger, E. Bouzy, J.S. Lecomte, EP a program for determination of crystallite orientations from TEM Kikuchi and CBED diffraction patterns, J. Appl. Crystallogr. 35 (2002), 287-287.

[46] C. Randau, U. Garbe, H.-G. Brokmeier, StressTextureCalculator: a software tool to extract texture, strain and microstructure information from area-detector measurements, J. Appl. Crystallogr. 44 (2011) 641 646.

[47] Y.D. Zhang, S.Y. Wang, C. Esling, J. Lecomte, C. Schuman, X. Zhao, L. Zuo, A method to identify dislocations in a known crystal structure by transmission electron microscopy, J. Appl. Crystallogr. 44 (2011) 1164 1168.

[48] S. Nag, R. Banerjee, R. Srinivasan, J.Y. Hwang, M. Harper, H.L. Fraser, ω-Assisted nucleation and growth of α precipitates in the Ti 5Al 5Mo 5V 3Cr 0.5Fe β titanium alloy, Acta Mater. 57 (2009) 2136 2147.

[49] M.J. Lai, T. Li, D. Raabe, ω phase acts as a switch between dislocation channeling and joint twinning- and transformation-induced plasticity in a metastable β titanium alloy, Acta Mater. 151 (2018) 67 77.

[50] J. Zhang, C.C. Tasan, M.J. Lai, A.C. Dippel, D. Raabe, Complexion-mediated martensitic phase transformation in Titanium, Nat. Commun. 8 (2017), 14210.

[51] Y.F. Zheng, R.E.A. Williams, G.B. Viswanathan, W.A.T. Clark, H.L. Fraser, Determination of the structure of α-β interfaces in metastable β-Ti alloys, Acta Mater. 150 (2018) 25 39.

[52] T. Li, D. Kent, G. Sha, L.T. Stephenson, A.V. Ceguerra, S.P. Ringer, M.S. Dargusch, J.M. Cairney, New insights into the phase transformation to isothermal ω and ω-assisted α in near β-Ti alloys, Acta Mater. 106 (2016) 353 366.

[53] J.R. Patel, M. Cohen, Criterion for the action of applied stress in the martensitic transformation, Acta Metall. 1 (1953) 531 538.

[54] D. De Knijf, T. Nguyen-Minh, R. Petrov, L.A.I. Kestens, J.J. Jonas, Orientation dependence of the martensite transformation in a quenched and partitioned steel subjected to uniaxial tension, J. Appl. Crystallogr. 47 (2014) 1261 1266.